https://doi.org/10.5194/egusphere-2026-1891
Preprint. Discussion started: 15 April 2026

Surface warming in the low-latitude Indo-Pacific Ocean during peak interglacials: A major challenge for Earth System Models

Martina Hollstein[1], Matthias Prange[1, 2], Lukas Jonkers[1], Mahyar Mohtadi[1, 2]

[1]MARUM - Center for Marine Environmental Sciences, University of Bremen, Bremen, Germany
[2]Faculty of Geosciences, University of Bremen, Bremen, Germany

Correspondence to: Martina Hollstein (mhollstein@marum.de)

Abstract. The tropical Indian and Pacific Oceans play a crucial role for global climate due to their extensive coverage across the low latitudes. However, our understanding of the regional sea surface temperature (SST) dynamics during major interglacial periods - when Earth's climate was warmer than the preindustrial period - remains limited. Here, we compare proxy-based SST reconstructions from the low-latitude Indo-Pacific with Community Earth System Model (CESM) simulations for three key interglacial intervals: the mid-Holocene, Marine Isotope Stage (MIS) 5e, and MIS 11c. Proxy data show an overall warming during MIS 5e and MIS 11c relative to the preindustrial period. Moreover, smaller zonal SST gradients across the equatorial Pacific indicate a weakening of the Pacific Walker circulation. We attribute these findings primarily to extratropical warming and its influence on ocean circulation, particularly the Atlantic Meridional Overturning Circulation and shallow meridional overturning circulation cells. In contrast, CESM simulations indicate lower-than-preindustrial SSTs during MIS 5e and MIS 11c peaks and a larger zonal gradient. We perform individual forcing experiments to disentangle the roles of orbital forcing, greenhouse gas concentration and vegetation cover in shaping SST anomalies. We find that the implementation of paleo-vegetation in CESM reduces the discrepancies between proxy and model data. However, it does not improve the zonal SST gradients, suggesting that model representations of tropical ocean and climate dynamics remain insufficient. Possible causes for these shortcomings are discussed. Our findings underscore the need for refined model physics and improved paleo-proxy integration to better simulate tropical climate behavior during interglacials.

1 Introduction

The low latitude oceans are central to global climate, driving global atmospheric circulation and the hydrological cycle. Among these, the low-latitude Indian and Pacific Oceans are particularly important due to their extensive coverage across the low latitudes. The Indo-Pacific Warm Pool (IPWP), the most dynamic region within the tropics with sea surface temperature (SST) above 28 °C, is a major source of heat and water vapor for the global atmosphere, driving deep atmospheric convection (Gagan et al., 2004) in the rising limb of the Hadley and Walker circulation cells. Spatiotemporal changes in SST of the IPWP alter the location and strength of atmospheric convection, affect the regional atmospheric and oceanic circulation systems (e.g., Fan et al., 2013), and eventually perturb the global atmospheric circulation (Neale and Slingo, 2003; Wang and Mehta, 2008). Recent climate simulations further suggest that the radiative response to surface warming of the western tropical Pacific is the dominant control on global radiative feedback changes (Dong et al., 2019).

Proxy-based reconstructions and climate model simulations provide ideal means to study the spatiotemporal SST variability and its underlying forcings on long time scales. Global compilations of interglacial SST anomalies and data – model comparisons have mostly focused on the Holocene (e.g. Schneider et al., 2010; Lohmann et al., 2013; Kaufman et al., 2020) and Marine Isotope Stage (MIS) 5e (~129 – 120 ka) (e.g. Hoffman et al., 2017; Otto-Bliesner et al., 2021; Turney et al., 2020; Mckay et al., 2011). For the low latitudes, although compilations of mid-Holocene (6 ka) mean annual temperature anomalies relative to the preindustrial (PI) period reveal a heterogenous picture, the pooled mean indicates that the mid-Holocene was slightly warmer, whereas climate models indicate cooler temperatures (e.g., Kaufman and Broadman, 2023; Brierley et al.,

https://doi.org/10.5194/egusphere-2026-1891
Preprint. Discussion started: 15 April 2026

2020; Kaufman et al., 2020). The following (mid- to late-Holocene) cooling trend inferred from the proxy records contradicts the warming simulated by climate models, which is commonly referred to as the 'Holocene Temperature Conundrum' (Liu et al., 2014).

For MIS 5e, both proxy-based compilations and climate models suggest cooler SSTs than during the PI period across large parts of the low-latitude ocean (e.g., Hoffman et al., 2017; Fischer et al., 2018; Otto-Bliesner et al., 2021). This is explained by a direct SST response to a reduced local mean annual insolation in combination with slightly lower greenhouse gas (GHG) concentrations (Hoffman et al., 2017), although the cooling inferred from proxy data is much stronger than the cooling in the models. For MIS 11c, global compilations of mean annual SST anomalies are not available yet. However, proxy and model-based SST reconstructions show inconsistent trends and variabilities (Milker et al., 2013). Due to the coupling between regional SSTs and atmospheric circulation, discrepancies between proxy- and model-based SST anomalies might lead to contrasting interpretations of past atmospheric and ocean circulation changes.

Overall, the mismatches between proxy-derived and simulated SST anomalies are ascribed to seasonal biases in the proxy reconstructions (e.g., Bova et al., 2021; Lohmann et al., 2013; Bader et al., 2020; Liu et al., 2014), and/or to model deficiencies, such as the insufficient representation of interglacial vegetation (e.g., Liu et al., 2018). Recently, Thompson et al. (2022) showed that the implementation of the paleo-vegetation into a Holocene simulation warms the Earth's surface (~0.7 °C at 6 ka) and provides a promising solution to the Holocene temperature conundrum as it gives rise to a mid-Holocene thermal maximum.

Despite its significance for global climate, the low-latitude Indo-Pacific is not covered well in available compilations of interglacial SST anomalies with little to no data from the IPWP. Here, we present a proxy network of SST anomalies from the low-latitude Indo-Pacific during mid-Holocene, MIS 5e and MIS 11c time slices. The selected periods were globally strong interglacials (Pages, 2016), i.e. periods of peak warmth, with comparable-to-preindustrial (PI) atmospheric GHG concentrations and ice volume, but with different astronomical configurations and thus insolation forcing (Fig. 1). The selected periods offer valuable testbeds to disentangle the roles of orbital forcing, GHG concentration and vegetation cover in shaping interglacial SSTs. By comparing the reconstructed SST anomalies with simulated anomalies of Community Earth System Model (CESM) 1.2.2 time slice simulations, we aim to explore to which degree a state-of-the-art model is able to capture interglacial tropical ocean dynamics and, whether discrepancies between reconstructed and simulated SSTs exist across different interglacials, and whether they can be resolved by implementation of an expanded NH vegetation cover.

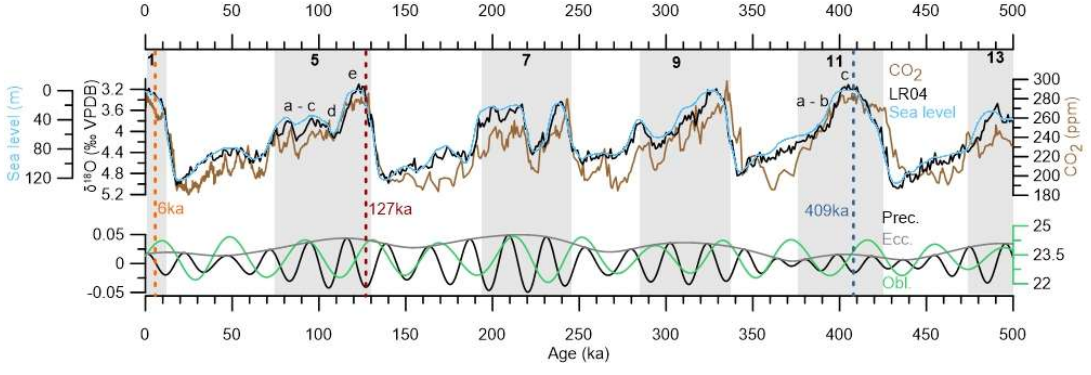

Figure 1: Reference records indicating changes in global climate (a) and astronomical forcing (b) during the past 500 kyr. (a) Benthic $\delta^{18}O$ stack record (black; Lisiecki and Raymo, 2005), sea level (blue; Bintanja and Van De Wal, 2008) and atmospheric CO_2 (brown; Bereiter et al., 2015). (b) Astronomical configuration showing precession (black), eccentricity (grey) and obliquity (green) (Laskar et al., 2004). Grey shadings mark interglacial periods. Colored vertical lines indicate the investigated time slices during the Holocene, MIS 5e and MIS 11c.

https://doi.org/10.5194/egusphere-2026-1891
Preprint. Discussion started: 15 April 2026

2 Methods

2.1 Compilation of SST records

Most SST reconstructions from the low-latitude Indo-Pacific are based on Mg/Ca and alkenone palaeothermometry and we limit our synthesis to these proxies. The Mg/Ca ratio in foraminifera tests has been the predominantly used proxy for SST reconstructions in the tropical Indo-Pacific. It is based on the thermodynamic effects on the incorporation of magnesium into the foraminifera tests during calcification and usually described with an exponential relationship (e.g., Rosenthal et al., 1997). The $U^{K'}_{37}$ index is based on the temperature dependent, relative unsaturation of long-chain (C_{37}) ketone lipids (alkenones) produced by coccolithophores (e.g., Brassell, 1986) and often used in the subtropical to high latitude Indo-Pacific.

We compiled a total of 137 records from the Indian and Pacific Oceans (45°N – 45°S; water depths between 61 and 5712 m) (Fig. 2, Table S1). Our compilation is based on the "PalMod 130k marine palaeoclimate data synthesis v2" (Jonkers et al., accepted). Notably, the PalMod data synthesis only includes sediment cores for which absolute age controls and / or benthic $\delta^{18}O$ records are available for chronology (for details see Sect. 2.2). To increase the spatial and temporal data coverage in this study, we additionally included eight cores for which only planktic (*G. ruber*) records are available.

We included Mg/Ca records that are based on *G. ruber albus* (Morard et al., 2019) and / or *G. elongatus (Aurahs et al., 2011)* (previously referred to as *G. ruber* s.s. and s.l., respectively). Assuming that the authors of the original data publications selected the most appropriate Mg/Ca-SST calibrations for their records, we retained these calibrations. For comparison, we additionally include SSTs calculated by the application of the global MgCarB calibration of Gray et al. (2018) as described in the PalMod synthesis (Jonkers et al., accepted) (see Text S1, Figs. S1 and S2). The MgCaRB calibration also accounts for the effects of salinity and pH on foraminiferal Mg/Ca. Likewise, to calculate alkenone-based SST anomalies, we applied the $U^{K'}_{37}$ -SST calibrations that were used in the original studies, but include SST estimates resulting from the application of the Bayesian BAYSPLINE calibration (Tierney and Tingley, 2018) in the supporting information (Text S1, Figs. S1 and S2).

Modern observations of the (intra) seasonal occurrence patterns of alkenone-producing coccolithophores and *G. ruber* are uncertain. Some studies do not reveal a clear pattern (e.g., Curry et al., 1992; Conan and Brummer, 2000; Kawahata et al., 2002; Yamasaki et al., 2008; Mohtadi et al., 2011), whilst others report different (intra) seasonal occurrence peaks of the proxy carriers (e.g., Mohtadi et al., 2009; Kincaid et al., 2000; Chen et al., 2007; Lin et al., 2004). For simplicity, we assume that the SST records from the study area represent mean annual SSTs, but discuss potential seasonal biases in Sect. 3.4.

2.2 Age models

The analysis of time slice data from various records requires robust chronologies and a common chronological framework for all records. We adopted the age-depth models of the PalMod data synthesis v2 (Jonkers et al., accepted) (see Text S2 for details). To generate the age-depth models of the cores for which benthic $\delta^{18}O$ records are not available, we also followed the approach of Jonkers et al. (accepted), but aligned the planktic $\delta^{18}O$ records to benthic $\delta^{18}O$ stack records. This approach ignores possible leads/lags between the surface and the deep ocean, but allows to use the same reference curves for all records of the data compilation. The PalMod age-depths models are restricted to the last 130 kyr. For MIS 11, we used the LR04 benthic stack (Lisiecki and Raymo, 2005) as reference record to align the $\delta^{18}O$ records. To quantify uncertainty, the chronologies were established in a Bayesian framework using the software Bacon (Blaauw and Christen, 2011). The age modelling routine was carried out in PaleoDataView (PDV; Langner and Mulitza, 2019). All ages are reported in 1000s of calendar years before present (ka BP).

https://doi.org/10.5194/egusphere-2026-1891
Preprint. Discussion started: 15 April 2026

2.3 Time slices

To assess SST anomalies during the Holocene, MIS 5 and MIS 11 peak interglacials relative to the preindustrial period, we calculated mean SST values of time slices centered at 6 ka (4–8 ka; 113 records), 127 ka (123–131 ka; 52 records) and 409 ka (405–413 ka; 13 records). The selection of the 6 and 127 ka time slices is consistent with the experiments of the paleoclimate model intercomparison project (PMIP). In comparison to the PI, the 6 ka time slice is characterized by higher obliquity and lower precession. The 127 and 409 ka time slices were selected to coincide with precession minima, maximizing astronomical forcing (Fig. 1) (Yin and Berger, 2011).

We used a Monte-Carlo approach to assess the combined age model and SST uncertainties. We generated 1,000 time series of SST using the posterior age–depth models and an assumed, Gaussian-distributed, SST uncertainty of 1 °C (1 σ) and calculated the 95 % confidence intervals of each record and time slice. The calculated confidence intervals range from an average of 0.7 °C for the mid-Holocene to an average of 1.3 °C for MIS 11c. We only included records with a minimum number of two SST data points within the respective time slice in at least 500 of the 1,000 age ensembles, as this number of posterior age–depth models proved sufficient to capture the chronological uncertainty. Because many proxy records do not cover the late Holocene (or even modern) period, we calculated SST anomalies relative to the long-term mean SSTs computed from the 1850–1900 monthly COBEv2 reanalysis data of the Japanese Meteorological Center (1.0 x1.0°; Hirahara et al., 2014) that are used as PI equivalent. This approach has the disadvantage that the SSTs of the reconstructed time slices and PI SSTs are not based on the same archive. To control the robustness of our results, we additionally calculated SST anomalies relative to the Common Era (CE) using all records covering the CE (total of 36 Mg/Ca and 24 $U^{K'}_{37}$ records; Fig. S4). Considering the reduced data coverage, we find that the overall outcome of this study does not depend on the choice of the PI dataset.

The reconstructed SST anomalies vary from site to site. To get a better idea of regional SST anomalies, we additionally calculated mean SST anomalies of three distinct areas, which are well represented by proxy records, i.e., the Western Pacific Warm Pool (WPWP), the South China Sea (SCS), and the eastern equatorial Pacific (EEP) (Fig. 2a, Table S4). Using a Markov Chain Monte Carlo sampling, we calculated weighted mean SSTs (weighted by the square root of the number of data points) of n randomly selected realizations of the time series within each area and time slice, where n equals the total number of SST records within the area and time slice. We repeat this 1,000 times and derive the median and 95 % confidence interval. By randomly sampling the records, we aim to consider spatial uncertainty. Likewise, by using weighted means, the resolution of the individual cores is considered. Anomalies were calculated relative to the COBE means of the sites included in each area and time slice.

2.4 Model configuration

For comparison with the proxy-based SST anomalies, we conducted time slice simulations using the CESM version 1.2.2 (Hurrell et al., 2013) (see Text S3 for details). The time slices were forced with constant boundary conditions, i.e., orbital parameters (Laskar et al., 2004) and atmospheric GHG concentrations (CO_2, CH_4 and N_2O) characteristic of the respective period (Table 1). GHG concentrations were obtained from Otto-Bliesner et al. (2017) or, for MIS 11c, from the European Project for Ice Coring in Antarctica (EPICA) following the AICC23 chronology (Bouchet et al., 2023). An adjustment of +23 ppb for methane was applied, following the experimental setup of previous interglacial modelling studies (Otto-Bliesner et al., 2017; Crow and Prange, 2025). Each time-slice simulation was branched from a PI control run as described in Crow et al. (2022), and integrated for 700 years to reach statistical equilibrium in the upper ocean. A key assumption in these simulations is the use of present-day topography, sea level, and ice-sheet configurations. All presented results are based on climatologies derived from the final 50 years of each simulation. SST anomalies are given relative to the PI simulation. Area mean SST

https://doi.org/10.5194/egusphere-2026-1891
Preprint. Discussion started: 15 April 2026

anomalies of the SCS, WPWP and EEP areas were calculated as mean anomalies of rectangles surrounding the included core sites (boundaries are provided in Table S4).

Table 1. Greenhouse gas concentrations used in the individual CESM runs

	CO_2 (ppm)	CH_4 (ppb)	N_2O (ppb)
PI	284	808	273
6 ka	264	597	262
127 ka	275	685	255
409 ka	280	700	275

To distinguish the effects of astronomical forcing and varying GHG concentrations on interglacial SST patterns, we additionally performed sensitivity experiments with fixed preindustrial GHG levels.

To assess the impact of NH vegetation changes on interglacial SSTs across the low-latitude Indo-Pacific Ocean, we conducted sensitivity experiments with an expanded vegetation cover. While in our standard interglacial time-slice simulations a preindustrial plant functional type (PFT) distribution is prescribed, we follow the approach of Thompson et al. (2022) in an additional mid-Holocene experiment in which C_3 grasses are replaced by boreal forest in the Arctic and by deciduous forest in mid-latitudes. In North Africa, shrub and C_4 grass replace bare ground, resulting in a green Sahara. Although global paleo-vegetation maps for previous interglacials are not available, similar vegetation shifts, including poleward expansion of trees at the expense of grasses in high northern latitudes as well as Sahara greening (Dupont, 1993), have been proposed for MIS 5e (CAPE, 2006; Otto-Bliesner et al., 2017 and references therein) and MIS 11c (Kleinen et al., 2014 and references therein). Therefore, we apply the PFT distribution of Thompson et al. (2022) as a generic interglacial vegetation scheme in additional sensitivity experiments for MIS 5e and 11c.

3 Results and Discussion

3.1 Reconstructed SST anomalies

Mg/Ca and $U^{K'}_{37}$ are preferentially used in different areas. While many Mg/Ca-derived SST reconstructions are available from the IPWP, SSTs from the northern and southern rims of the study area are mostly derived from $U^{K'}_{37}$. Comparing Mg/Ca- and $U^{K'}_{37}$-derived SST estimates from sites where both proxies are available, previous studies find that there is no systematic offset (e.g., Hoffman et al., 2017). We observe higher (i.e., warmer) $U^{K'}_{37}$-derived SST anomalies as compared to Mg/Ca-based SST estimate Southern Hemisphere sites, and lower (i.e., cooler) $U^{K'}_{37}$-derived SST anomalies at northern Hemisphere sites (Fig. S5). This could indicate a winter (cold year) bias of $U^{K'}_{37}$ and/or summer (warm year) bias of Mg/Ca, which will be discussed in more detail in Sect. 3.4. Importantly, this offset does not impact the overall outcome of this study.

During the 6 ka time slice, both Mg/Ca and $U^{K'}_{37}$ reveal a spatially heterogeneous pattern of SST anomalies across the low latitude Indo-Pacific (Fig. 2a). Records from western Indian and most of the Pacific Ocean depict positive SST anomalies (i.e., higher mid-Holocene SSTs as compared to the PI), except for the northeastern Pacific Ocean, which depicts negative SST anomalies. Records from the northern Indian Ocean show both positive and negative anomalies, and most records from the eastern Indian Ocean and the Indonesian Seas indicate negative mid-Holocene SST anomalies. Computed mean anomalies for the SCS, WPWP and EEP areas are negligible (median values of ±0.1 °C; Fig. 3) in line with the general pattern of smaller

https://doi.org/10.5194/egusphere-2026-1891
Preprint. Discussion started: 15 April 2026

anomalies in the tropics and larger anomalies towards the northern and southern margins of the study area, i.e., the mid-latitudes (Fig. 2, Table S4). Overall, our results agree with previous multiproxy mid-Holocene SST compilations (e.g., Kaufman and Broadman, 2023; Lohmann et al., 2013).

The MIS 5e is characterized by positive SST anomalies (up to 3.6 °C, average 0.8 °C) at nearly all sites with maximal values at the northern and southern margins of the western Pacific Ocean and in the EEP (Fig. 2c and d). The average SST anomaly of the EEP is ~1.9 °C, while the anomalies of the SCS and WPWP areas are ~0.7 °C and ~0.8 °C, respectively (Fig. 3). Our MIS 5e data are consistent with previous compilations, such as the multi-proxy compilation of Turney et al. (2020), although the inclusion of microfossil proxies leads to a larger variety of SST anomalies (Fig. S6). The data compilation indicates that MIS 11c is also characterized by higher SSTs (up to 2.1 °C, average 0.9 °C) than the PI (Fig. 2e). Similar to MIS 5e, the SST anomaly of the EEP is larger (~2.0°C) than the SST anomalies of the SCS and WPWP areas (~0.5 °C) (Fig. 3).

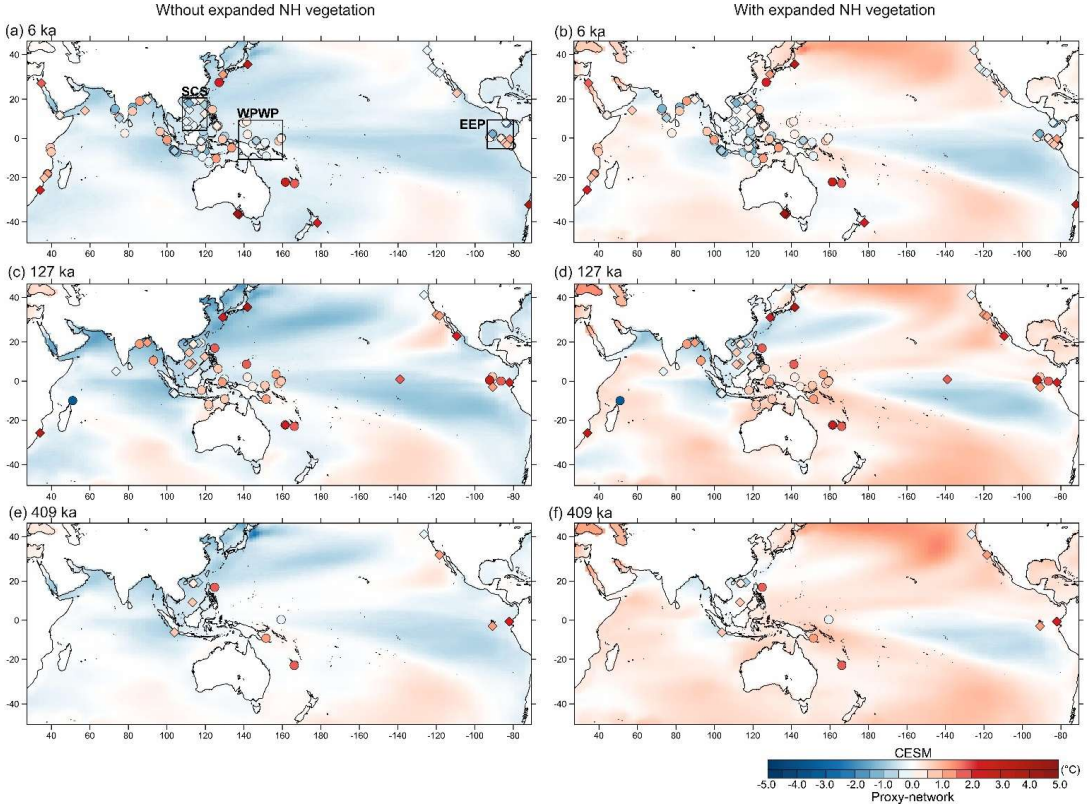

Figure 2: SST anomalies during (a, b) Mid-Holocene, (c, d) MIS 5e, and (e, f) MIS 11c relative to the preindustrial period from Community Earth System Model (CESM) 1.2.2. time slice simulations without (a, c, e) and with (b, d, f) expanded NH vegetation. Symbols represent Mg/Ca- (dots) and $U^{K'}_{37}$ -(diamonds) based SST anomalies relative to COBEv2 1850-1900 SST. Colors indicate SSTs colder (blue) and warmer (red) than the reference period.

Very few datasets in our compilation cover MIS 11c, with only one record from the Indian Ocean. However, records covering both periods indicate a high similarity between the MIS 5e and MIS 11c. The same is true for the calculated mean SST anomalies of the WPWP, SCS and EEP areas. The reconstructed SST anomalies represent conservative estimates of peak warmth. This is because the selected time slices may not coincide with the timing of maximum SSTs at the individual core sites, and averaging SSTs tends to dampen peak values and underestimate the true magnitude of peak interglacial SSTs.

https://doi.org/10.5194/egusphere-2026-1891
Preprint. Discussion started: 15 April 2026

Different SST anomalies for the WPWP relative to the EEP result in a reduced or an increased zonal equatorial Pacific thermal gradient - a key driver of the Pacific Walker circulation. Proxy data indicate no major difference in the equatorial Pacific SST gradient (~0.2°C) between 6 ka and the PI. The 127 ka and 409 ka time slices are marked by reductions of ~1.1 °C and ~1.5 °C, respectively (Fig. 4; Table S4). This should be interpreted with caution due to the partly very low number of records included in the area mean anomalies, but is consistent with previous reconstructions indicating an increased gradient during the mid-Holocene (e.g., Koutavas et al., 2002; Marchitto et al., 2010) and a reduction during MIS 5e (Jia et al., 2018; Sagawa et al., 2022). We thus find that overall higher SSTs during MIS 5e and MIS 11c are associated with a weaker Walker circulation. This finding conflicts with previous studies (e.g. Hollstein et al., 2020; Jian et al., 2022; Lo et al., 2022; Zhang et al., 2021; Pena et al., 2008; Lu et al., 2019) that suggest a stronger Walker circulation (or more La Niña-like conditions) during periods of low precession. However, most of these studies are either based solely on model simulations or rely on reconstructions from only one side of the tropical Pacific, limiting their ability to constrain the zonal pattern of SST anomalies.

Together, our SST proxy compilation shows that the mid-Holocene was broadly similar to the PI reference period. In contrast, both MIS 5e and MIS 11c were consistently warmer than PI conditions across the entire study area, despite lower mean annual insolation at low latitudes and reduced GHGs. Hence, the warm anomalies are not related to local insolation forcing and varying GHGs, but to the astronomically modulated distribution of insolation and its feedback mechanisms. The three investigated time slices are marked by higher obliquity and lower precession than the PI with precession minima during 127 ka and 409 ka (Fig. 1). Sensitivity to obliquity and precession is known from many individual SST records of the study area (e.g., Tachikawa et al., 2014; Hollstein et al., 2020; Lo et al., 2022; Lückge et al., 2009; Pena et al., 2008; Wang et al., 2015; Gebregiorgis et al., 2018) that report higher SST under high obliquity and low precession. While local effects might also play a role - such as precession-controlled changes in upwelling intensity (Lückge et al., 2009) - the consistency of surface ocean warming across the entire study area points to common forcings. Focusing on the tropical Pacific Ocean, we suggest that the SST rise and the simultaneous slowdown of the Walker circulation were controlled by remote effects of extratropical / high latitude warming and ice loss and their effects on the Atlantic Meridional Overturning Circulation (AMOC) and the shallow meridional overturning circulation, as well as changes in the (seasonal) local insolation.

Warming of the high latitudes and (sea) ice loss could drive tropical warming and weaken the Pacific Walker circulation via both atmospheric and oceanic pathways, as it is suggested for the current global warming by theoretical considerations and idealized models (e.g., England et al., 2020). These pathways include a slowdown of the AMOC that results from lowered surface salinity in the North Atlantic and reduced deepwater formation and a slowdown of the subtropical shallow meridional overturning circulation cells that is controlled by surface wind anomalies over the subduction zones (England et al., 2020).

The AMOC state during previous interglacials is uncertain and debated: A recent modelling study suggests a moderate weakening of the AMOC during peak MIS 5e and MIS 11c attributed to sea ice minima (Crow and Prange, 2025). More generally Toggweiler and Si (2025) hypothesize that a weak AMOC during precession minima leads to an overall warming of the tropics of both hemispheres through a reduction in the cold-water upshifts of the AMOC's return flow. Particularly, maximal boreal summer insolation causes a relaxation of the easterly winds over the tropical Atlantic, which prevents the export of moisture from the Atlantic to the Pacific and leads to a freshening of the Atlantic. At the same time, less surface water is piled up in the West Atlantic. Both results in a weakening of the AMOC including its return flow and upshifts of cool waters to the surface off Peru. Less cool waters are incorporated into the shallow overturning circulation. This could primarily promote warming of the EEP and result in a reduced zonal SST gradient across the equatorial Pacific Ocean.

Positive SST anomalies in the low latitudes could additionally result from changes in the shallow meridional overturning circulation. Generally, higher obliquity results in a reduced mean annual insolation in the low latitudes, but an increasingly enhanced insolation towards the poles, in line with the latitudinal pattern that we observe in the western Pacific Ocean with a stronger warming towards higher latitudes. Hence, higher obliquity causes a reduced intrahemispheric (equator–pole)

https://doi.org/10.5194/egusphere-2026-1891
Preprint. Discussion started: 15 April 2026

insolation and surface pressure (and ultimately temperature) gradient that results in a reduced transport of warm waters out of the tropics by western boundary currents and thus, accumulation of heat there (e.g., Bosmans et al., 2015; Mantsis et al., 2011). Previous studies indicated that the warming is not evident at the sea surface (e.g., Hollstein et al., 2018; Mantsis et al., 2011). However, the response to changes in obliquity could be intensified by feedbacks, such as cloud and albedo / sea-ice albedo feedbacks (Bosmans et al., 2015; Mantsis et al., 2011; Timmermann et al., 2014b). This effect could be maximized when high obliquity coincides with precession minima, as it is the case at 127 ka and 409 ka. Surface waters of the equatorial Pacific Ocean are mostly sourced from the extratropical South Pacific, where surface waters are predominantly subducted during austral winter (Qu et al., 2013). A warmer austral winter and cooler, but prolonged austral summer during periods of low precession could result in the transport of relatively warmer subtropical waters towards the equatorial Pacific Ocean. Because the water masses resurface in the eastern Pacific Ocean, the warming of the EEP might be stronger than the warming of the WPWP and Indonesian Seas, reducing the zonal equatorial Pacific SST gradient and weakening the Pacific Walker circulation.

Weakening of the Walker circulation at 127 and 409 ka may result from changing SST gradients along with the overall global warming (Held and Soden, 2006). In addition, precession-controlled variations in the local fall (Sept-Oct) insolation and related zonally asymmetric heating of the equatorial Pacific -resulting from the northern position of the ITCZ in the EEP at this time and the associated wind field convergence in the west and divergence in the east - impacts the zonal SST gradient (Clement et al., 1999). A weaker fall insolation at 127 ka and 409 ka, as compared to the PI, would contribute to a reduced zonal equatorial Pacific SST gradient and Pacific Walker circulation. However, this hypothesis remains controversial and is not supported by records that cover multiple glacial-interglacial cycles (Dyez et al., 2016).

Global proxy-based SST compilations also indicate higher mean SSTs during the MIS 5e period relative to the PI (e.g., Turney et al., 2020; Mckay et al., 2011; Otto-Bliesner et al., 2021; Hoffman et al., 2017). However, this warm anomaly mainly results from warmer SSTs at mid- and high latitudes, while the tropical ocean is reported to have been cooler. This is due to cooler SSTs in the tropical Atlantic Ocean, which is prominently represented in these compilations (Hoffman et al., 2017; Turney et al., 2020). However, the Atlantic records in these compilations are mostly derived from foraminiferal assemblage transfer functions, which yield cooler SSTs, resulting in negative SST anomalies, whereas Mg/Ca and $U_{37}^{K'}$ records mostly show positive SST anomalies (e.g., Nascimento et al., 2023; Hoffman et al., 2017; Turney et al., 2020; Brocas et al., 2019). Thus, the tropical Atlantic Ocean could have been warmer during MIS 5e than inferred from the global proxy data compilations (see also Nascimento et al., 2022). In any case, our findings underscore the importance of including records from the Indian and Pacific Oceans in tropical and global climate data syntheses, as previous studies are biased towards the Atlantic Ocean and assemblage-based reconstructions.

3.2 Simulated SST anomalies

The simulated annual mean SST anomalies are small with maximum values of about 2 °C relative to the PI run (Fig. 2). CESM indicates cooler than preindustrial SSTs across large parts of the study area for all three investigated interglacial periods (Figs. 2 and 3). Exceptions are the eastern Pacific between 15°N and 45°N and the central Indian and Pacific Oceans south of 15°S, which are slightly warmer than the PI equivalent (Fig. 2). Overall, the mid-Holocene time slice is marked by the smallest SST anomalies. Mean SST anomalies of the SCS, WPWP and EEP areas range between -0.5 and -0.3 °C (Table S4). During MIS 5e and MIS 11c, the SST anomalies are generally larger. This refers to both positive and negative SST anomalies. Both periods are characterized by extended areas of higher SSTs in the southern parts of the study area and in the northeastern Pacific Ocean as compared to the mid-Holocene period. Mean anomalies of the SCS, WPWP and EEP areas range from -0.8 to 0.0 °C (Table S4). MIS 11c is warmer than the mid-Holocene and MIS 5e, albeit cooler than the PI equivalent across large parts of the study area (Fig. 2 and Fig. S7). The general spatial patterns of the SST anomalies during 6 ka and 127 ka simulations are in agreement

https://doi.org/10.5194/egusphere-2026-1891
Preprint. Discussion started: 15 April 2026

with the spatial patterns of previous simulations, such as the CMIP6-PMIP4 multi-model ensemble (Otto-Bliesner et al., 2021; Brierley et al., 2020). However, the standard simulations indicate a subtle increase (<0.2 °C) in SST gradients during the 6 ka and 409 ka time slices, as compared to the PI period and a negligible decrease (<0.1 °C) during the 127 ka time slice. In contrast, the PMIP4-CMIP6 ensemble yields a slight decrease in the mid-Holocene gradient (Brierley et al., 2020).

In CESM, the SST anomalies result from the combined effects of changing orbital parameters and GHG concentrations (Figs. S8 and S9). Sensitivity experiments with fixed (PI) GHGs show that varying orbital parameters result in extended areas of positive SST anomalies during the investigated time slices, supporting our proxy-based interpretation of SST anomalies. Despite the relatively small changes, adjusted GHG concentrations result in cooler conditions across the low-latitude Indo-Pacific during the 6 ka experiment, which is marked by lowest GHG concentrations (Table 1) (Figs. S8). The 127 ka experiment indicates that reduced GHG concentrations result in cooler SSTs over the vast Indian and Pacific Oceans, but in a slight warming near the Australasian landmasses and within the north Pacific Subtropical Gyre. Similarly, reduced GHG concentrations results in a slight warming across large parts of the western Pacific and some patches of the northern Indian Ocean in the 409 ka experiment, suggesting a dominant role of negative GHG feedbacks in these areas. While the 127 ka time slice is the warmest of the three interglacial period in the single-forced experiment, the 409 ka period is the warmest period, when dynamic GHGs are implemented. Overall, the results demonstrate that the low-latitude Indo-Pacific Ocean is most sensitive to small changes in the radiative forcing, but GHGs effectively modulate interglacial SSTs.

The sensitivity experiments with an expanded NH vegetation cover result in warmer SSTs across large parts of the low-latitude Indo-Pacific Ocean (as compared to the standard simulations) in all three time slice simulations (Fig. 2, Fig. S10). A subtle cooling trend (<0.2 °C) is evident in the upwelling zone of the eastern tropical Pacific Ocean during the mid-Holocene. In the SCS, WPWP and EEP areas, the average vegetation effect is between 0.2 and 0.7 °C (Table S4). A larger effect is observed in the NH mid-latitudes, where SSTs warm by a maximum of 3.4 °C (Fig. S10). As outlined in Thompson et al. (2022) the global-scale surface warming is mainly attributable to vegetation-induced changes in surface albedo.

CESM indicates a subtle increase (<0.3 °C) in the zonal equatorial Pacific (WPWP – EEP) SST gradient during all time slices, as compared to the PI period, except for the 127 ka time slice standard simulation (Fig. 4). This results from the simulated cooling in the eastern Pacific upwelling zones. The implementation of paleo-vegetation results in an increase of ~0.2–0.4 °C in the zonal SST gradient during all time slices. Hence, the relative increase in SST gradients is larger in the experiments that consider paleo-vegetation.

3.3 Proxy data – model comparison

We observe large discrepancies concerning both magnitude and pattern of SST change (Fig. 2). Overall, the annual mean SST anomalies in CESM are smaller than indicated by proxy reconstructions. Underestimation of interglacial temperature anomalies in climate models is a well-known, persisting issue (e.g., Brierley et al., 2020; Milker et al., 2013; Otto-Bliesner et al., 2021). More importantly, reconstructed and simulated anomalies are mostly of opposite sign. Proxy-data indicate SSTs above the PI values for MIS 5e and MIS 11c, whereas CESM standard simulations indicate SSTs below the PI values at most of the proxy sites (Fig. 2a, c, e). In CESM, MIS 11c is the warmest of the three investigated interglacial periods, albeit cooler than the reference period. Consistent trends between proxies and CESM exist mainly for the northeastern Pacific Ocean and the Solomon-Coral Sea, where both the proxy network and CESM indicate slightly warmer-than-preindustrial SSTs, particularly during the MIS 5e and MIS 11c time slices. However, also for these areas, the magnitude of SST anomalies in CESM is smaller than indicated by proxy data.

When implementing the paleo-vegetation in CESM simulation, a quantitatively small yet consistent warming improves the match between reconstructed and simulated SST anomalies (Figs. 2b, d, f and 3). However, the magnitude of the simulated

https://doi.org/10.5194/egusphere-2026-1891
Preprint. Discussion started: 15 April 2026

SST anomalies is still smaller than the reconstructed anomalies. Despite the discrepancies between the reconstructed and simulated SST anomalies, the mid-Holocene and MIS 11c area means of the SCS, WPWP and EEP calculated from the CESM output (standard simulations and vegetation experiments) fall mostly within the estimated uncertainty range of the proxy reconstructions (Fig. 3). This is because the individual mid-Holocene proxy-based anomalies are negligibly small and of no clear sign. During MIS 11c, proxy-based reconstructions have a higher uncertainty, which is primarily related to the increased uncertainties of the age models and the small number of SST records that are available in each of the areas.

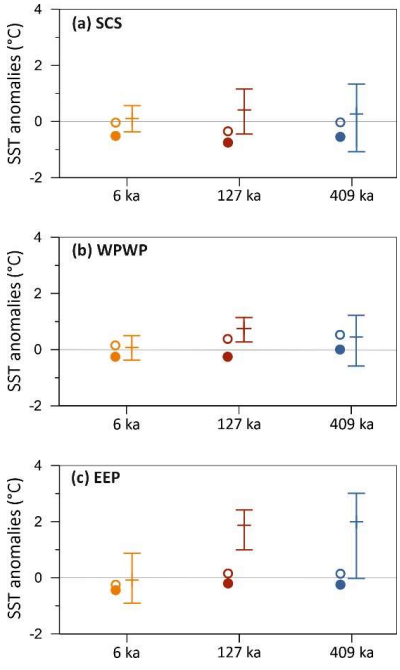

Figure 3: Comparison between interglacial proxy- and model-based SST anomalies in (a) the SCS, (b) the WPWP and (c) the EEP. Bars indicate proxy-based assessments of computed mean SST anomalies and uncertainties (shown as median and 95 % confidence intervals), dots indicate SST anomalies derived from CESM runs without (filled) and with (open) expanded vegetation cover. The SCS, WPWP and EEP areas are marked by black rectangles in Fig. 2a.

The different SST anomalies lead to contrasting inferences about the atmospheric circulation. As outlined above, reconstructions indicate a reduction in the zonal equatorial Pacific SST gradient and thus, a weaker Walker circulation during MIS 5e and MIS 11c, while CESM indicates the opposite (Fig. 4; Table S4). Notably, the implementation of paleo-vegetation in CESM results in an increase of ~0.2–0.4 °C in the zonal SST gradient during all time slices. Thus, the paleo-vegetation improves the overall match of absolute SST anomalies, whereas discrepancies in the spatial patterns of SST anomalies remain.

Overall, our findings suggest that a “temperature conundrum” also exists during MIS 5e and MIS 11c, as model temperatures are colder than reconstructions during the peak interglacials. An expanded NH vegetation affects the interglacial SST anomalies by changing their sign from negative to positive anomalies, and is thus critical to be considered in interglacial climate simulations. However, although the simulations represent the high end of a potential interglacial vegetation expansion and resulting temperature response (Thompson et al., 2022; Kaufman and Broadman, 2023), differences in the magnitude of SST anomalies persist. Besides, the expanded vegetation enhances the mismatch between reconstructed and simulated zonal equatorial Pacific SST gradients with implications for inferred changes in the atmospheric circulation and El Niño-Southern Oscillation (ENSO) dynamics. Hence, the implementation of an interglacial vegetation scheme cannot solve the data-model

https://doi.org/10.5194/egusphere-2026-1891
Preprint. Discussion started: 15 April 2026

discrepancies. Alternatively, discrepancies can result from seasonal or interannual proxy biases, which we address in Sect. 3.4. In Sect. 3.5 we then focus on potential model deficiencies.

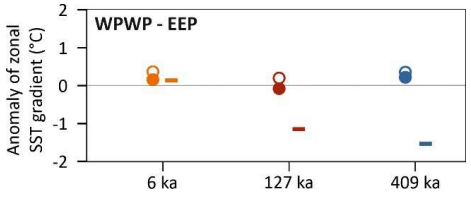

Figure 4: Anomalies of zonal equatorial Pacific SST gradients during mid-Holocene (orange), MIS 5e (red) and MIS 11c (blue) time slices relative to the preindustrial period. Bars indicate reconstructed anomalies, dots indicate SST anomalies derived from CESM runs without (filled) and with (open) expanded vegetation cover.

3.4 Potential seasonal or interannual proxy biases

We assume that proxy reconstructions reflect annual mean SSTs across the study area, though potential (intra) seasonal imprints on Mg/Ca and $U_{37}^{K'}$-derived SST records are not entirely understood yet. Some reconstructions, partly based on records that we included in our data compilation, suggest that Mg/Ca and $U_{37}^{K'}$ record different seasons (Leduc et al., 2010; Timmermann et al., 2014a; Wang et al., 2013), at least in parts of the study area. For instance, in the EEP, $U_{37}^{K'}$ may record boreal winter SST, while Mg/Ca records may record mean annual to summer SST (Leduc et al., 2010). This is consistent with the Northern and Southern Hemisphere offsets between Mg/Ca and $U_{37}^{K'}$ that we observed (see Sect. 3.1).

A potential preference of the proxy carriers towards the warm season has also been used to explain discrepancies between reconstructions and simulations (e.g., Bova et al., 2021). Others suggest that summer conditions persist into the fall and winter in response to feedbacks and slow-moving features of the climate system and thus, mean annual temperature could be dominated by strong changes in summer (Zhang et al., 2010; Bader et al., 2020; Kaufman and Broadman, 2023).

In order to further test if a warm season bias of the proxy records would reasonably explain the observed data-model discrepancies, we compare the proxy-based mean area SST anomalies of the SCS, WPWP and EEP to the corresponding seasonal SST anomalies, i.e. minimum and maximum SST, inferred from CESM (Fig. 4). We find that the majority of both Mg/Ca and $U_{37}^{K'}$-based SST anomalies exceeds the simulated warm-season SST anomalies (Fig. 5). This is especially true for SST anomalies in the standard simulation, i.e. without expanded NH vegetation. The implementation of paleo-vegetation does not alter the seasonal cycle, but results in higher SSTs year-round, partly improving the match between seasonal SSTs and proxy-SSTs.

Moreover, the difference in the SST anomalies between MIS 5e and MIS 11c is negligible, despite the weaker astronomical forcing during MIS 11c. A damped precession and lower obliquity should subdue seasonal insolation cycle during MIS 11c, eventually affecting seasonal SSTs.

https://doi.org/10.5194/egusphere-2026-1891
Preprint. Discussion started: 15 April 2026

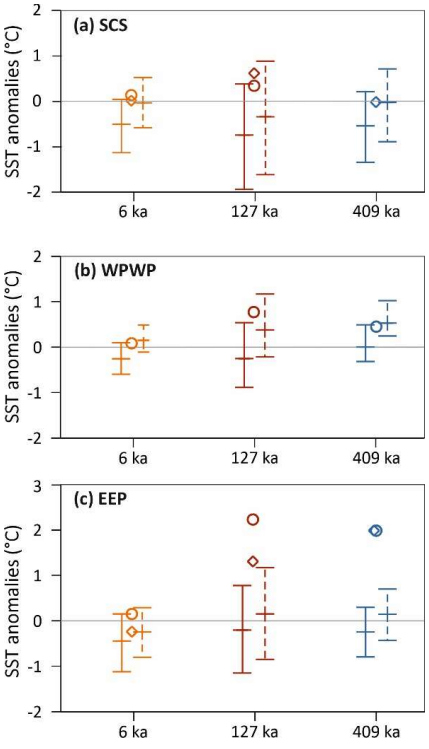

Figure 5: Comparison between reconstructed and simulated SST anomalies in the (a) South China Sea (SCS), (b) Western Pacific Warm Pool WPWP) and (c) eastern equatorial Pacific (EEP) during mid-Holocene (orange), MIS 5e (red) and MIS 11c (blue) time slices relative to the preindustrial period. Bars indicate mean, minimum and maximum annual SST anomalies in CESM without (solid lines) and with (stippled lines) expanded NH vegetation cover. Symbols represent Mg/Ca- (dots) and $U_{37}^{K'}$ - (diamonds) based SST anomalies. The SCS, WPWP and EEP areas are marked by black rectangles in Fig. 2a.

In order to test if interannual variability, i.e. a bias towards warm years in the proxies, can potentially explain the observed proxy data-model discrepancy, we calculated the standard deviation of mean annual SSTs in CESM. CESM indicates a reduced standard deviation and, thus, a reduced interannual variability relative to PI in most regions of the low-latitude Indo-Pacific during all investigated time slices, particularly when interglacial vegetation cover is implemented (Fig. 6). A warm-year bias in the proxies would equally affect the reconstructed reference SSTs of the CE and those of previous interglacials if interannual variability was unchanged. However, the warm-year bias would be smaller for the previous interglacials given the reduced interannual variability indicated by CESM. Hence, a warm-year bias in the proxies is unlikely to explain the data–model discrepancy.

Taken together, although consideration of a potential seasonal bias in the proxies improves the match between data and model, we find that biases to warm seasons or years could not resolve the data–model discrepancy overall. This does not negate potential seasonal or interannual proxy biases and related discrepancies between $U_{37}^{K'}$ and Mg/Ca in different regions, but suggests that the overall signal, i.e. positive SST anomalies during MIS 5e and MIS 11c, that is observed in both proxies across the entire study area, is a robust feature that is not simply attributable to seasonal or interannual proxy biases.

https://doi.org/10.5194/egusphere-2026-1891
Preprint. Discussion started: 15 April 2026

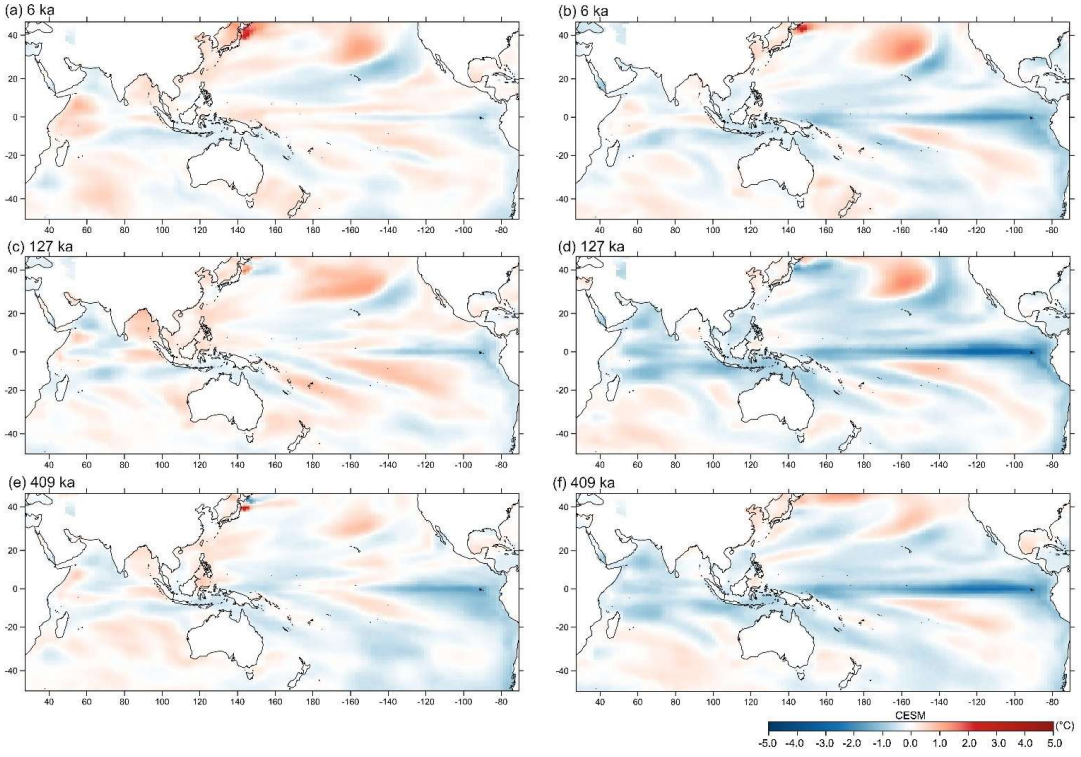

Figure 6: Standard deviation of mean annual SSTs during (a, b) Mid-Holocene, (c, d) MIS 5e, and (e, f) MIS 11c relative to the preindustrial period from CESM time slice simulations without (a, c, e) and with (b, d, f) expanded northern hemisphere vegetation. Blueish and reddish colors indicate decreased and enhanced standard deviations, respectively.

3.5 Potential model deficiencies

The discussed AMOC changes are uncertain and require further investigations. However, an insufficient representation of the AMOC's return flow (Toggweiler and Si, 2025), and of past AMOC variations and their effects in global models such as CESM could at least partially explain the data–model discrepancies. Regardless of what a change in the AMOC may have caused, the resolution of typical global climate models such as CESM is too coarse to simulate the effect of reduced cold-water upshifts on tropical warming. CESM indicates a slight AMOC reduction at 127 and 409 ka (Crow and Prange, 2025). This reduction might be underestimated due to an inaccurate ice sheet forcing, or a systematic overestimation of AMOC stability (Liu et al., 2017). Inaccuracies in the representation of the ocean circulation, such as poorly simulated upshifts of cool waters (Toggweiler and Si, 2025), could result in an underestimation of warming (or even in a cooling) in the EEP and affect the Walker circulation. The accurate representation of the Walker circulation is generally a major challenge for climate models. Comparisons of observations and simulations of the last century show that models fail to reproduce the currently observed strengthening of the Walker circulation (e.g., Watanabe et al., 2023 and references therein).

Additional well known, but persistent model deficiencies include the insufficient representation of clouds and cloud feedbacks in response to warming and cooling. Uncertainties in cloud feedbacks is the largest contributing factor to the varying responses of models to GHG forcing (e.g., Soden and Held, 2006; Zelinka et al., 2020), and were shown to affect meridional and zonal temperature gradients and deep atmospheric convection in the tropics (Erfani and Burls, 2019).

https://doi.org/10.5194/egusphere-2026-1891
Preprint. Discussion started: 15 April 2026

4 Summary and conclusions

We provide a proxy data–model synthesis of interglacial SST anomalies (mid-Holocene, MIS 5e and MIS 11c) across the low-latitude Indo-Pacific Ocean. While the proxy compilation indicates negligible mid-Holocene SST anomalies of conflicting sign, the regional SSTs during MIS 5e and MIS 11c were generally higher than during the PI. Reduced zonal equatorial Pacific SST gradients additionally indicate a weakening of the Pacific Walker circulation. Changes in SST (gradients) are mainly ascribed to an enhanced extratropical warming and (sea) ice loss that affect the tropical ocean via changes in the AMOC and the shallow overturning circulation. A weaker local fall insolation during precession minima could additionally influence the zonal SST gradient via its effect on the ITCZ position and the wind field.

Our results challenge previous global proxy data compilations and tropical SST stack records that indicate cooler SSTs during the last peak interglacial MIS 5e. However, these compilations are biased towards foraminiferal assemblage records from the Atlantic. While proxy networks always suffer from an uneven spatial coverage and proxy-dependent limitations, our results highlight the need to integrate Indo-Pacific data into future (tropical or global) climate data syntheses and stack records to better capture low-latitude climate variability.

We find large discrepancies in the magnitude and spatiotemporal pattern of reconstructed and modeled SST anomalies, suggesting that a “temperature conundrum” is a persisting issue during several interglacial periods. Most importantly, proxy data indicate higher than preindustrial SSTs and a weakened equatorial gradient during MIS 5e and MIS11c, whereas CESM indicates the opposite. We find that the implementation of a paleo-vegetation scheme, i.e., an expanded Northern Hemisphere vegetation, in CESM has a significant impact on modelled SSTs, as it yields warmer SSTs across the vast tropical Indo-Pacific, improving the match between proxy and model-based SST anomalies during the investigated interglacial periods. The accurate representation of paleo-vegetation in climate models is thus critical to be considered in future climate simulations. However, discrepancies between reconstructed and simulated zonal SST gradients remain with important implications for the atmospheric circulation and the state of ENSO.

Data–model discrepancies might be resolved through improved proxy calibrations using modern regional time series and through a more accurate representation of tropical ocean and climate processes in models such as cold-water upshifts and cloud feedbacks.

Data availability

The PalMod data synthesis v2 (Jonkers et al., accepted) used in this study is publicly available at PANGAEA via https://doi.org/10.1594/PANGAEA.984602. We will additionally provide age models that are not part of the PalMod data synthesis on zenodo. The code that we used to calculate area mean SSTs and uncertainties will be provided at Zenodo. COBE-SST 2 data are from the Japanese Meteorological Center (JMA; Hirahara et al., 2014) provided by the NOAA PSL, Boulder, Colorado, USA, at their website at https://psl.noaa.gov.

Author contributions

MH: Conceptualization, Formal analysis, Visualization, Writing – original draft
MP: Conceptualization, Model simulations, Formal analysis, Writing – review & editing, Funding acquisition
LJ: Formal analysis, Writing – review & editing,
MM: Conceptualization, Writing – review & editing, Funding acquisition

https://doi.org/10.5194/egusphere-2026-1891
Preprint. Discussion started: 15 April 2026

Competing interests

At least one of the (co-)authors is a member of the editorial board of Climate of the Past.

Disclaimer

Copernicus Publications adds a standard disclaimer: "Copernicus Publications remains neutral with regard to jurisdictional claims made in the text, published maps, institutional affiliations, or any other geographical representation in this paper. While Copernicus Publications makes every effort to include appropriate place names, the final responsibility lies with the authors. Views expressed in the text are those of the authors and do not necessarily reflect the views of the publisher."

Please feel free to add disclaimer text at your choice, if applicable.

Acknowledgements

This study was funded by the Deutsche Forschungsgemeinschaft (DFG, German Research Foundation), Cluster of Excellence "The Ocean Floor— Earth's Uncharted Interface" (EXC 2077, grant no. 390741603).

References

Aurahs, R., Treis, Y., Darling, K., and Kucera, M.: A revised taxonomic and phylogenetic concept for the planktonic foraminifer species *Globigerinoides ruber* based on molecular and morphometric evidence, Marine Micropaleontology, 79, 1–14, https://doi.org/10.1016/j.marmicro.2010.12.001, 2011.

Bader, J., Jungclaus, J., Krivova, N., Lorenz, S., Maycock, A., Raddatz, T., Schmidt, H., Toohey, M., Wu, C.-J., and Claussen, M. C.: Global temperature modes shed light on the Holocene temperature conundrum, Nature communications, 11, 10.1038/s41467-020-18478-6, 2020.

Bereiter, B., Eggleston, S., Schmitt, J., Nehrbass-Ahles, C., Stocker, T. F., Fischer, H., Kipfstuhl, S., and Chappellaz, J.: Revision of the EPICA Dome C CO_2 record from 800 to 600 kyr before present, Geophysical Research Letters, 42, 542–549, https://doi.org/10.1002/2014gl061957, 2015.

Bintanja, R. and Van de Wal, R. S.: North American ice-sheet dynamics and the onset of 100,000-year glacial cycles, Nature 454, 869–872, https://doi.org/10.1038/nature07158, 2008.

Blaauw, M. and Christen, J. A.: Flexible Paleoclimate Age-Depth Models Using an Autoregressive Gamma Process, Bayesian Analysis, 6, 457–474, https://doi.org/10.1214/11-ba618, 2011.

Bosmans, J. H. C., Hilgen, F. J., Tuenter, E., and Lourens, L. J.: Obliquity forcing of low-latitude climate, Climate of the Past, 11, 1335–1346, https://doi.org/10.5194/cp-11-1335-2015, 2015.

Bouchet, M., Landais, A., Grisart, A., Parrenin, F., Prié, F., Jacob, R., Fourré, E., Capron, E., Raynaud, D., Lipenkov, V. Y., Loutre, M.-F., Extier, T., Svensson, A., Legrain, E., Martinerie, P., Leuenberger, M., Jiang, W., Ritterbusch, F., Lu, Z.-T., and Yang, G.-M.: The Antarctic Ice Core Chronology 2023 (AICC2023) chronological framework and associated timescale for the European Project for Ice Coring in Antarctica (EPICA) Dome C ice core, Climate of the Past, 19, 2257–2286, https://doi.org/10.5194/cp-19-2257-2023, 2023.

Bova, S., Rosenthal, Y., Liu, Z., Godad, S. P., and Yan, M.: Seasonal origin of the thermal maxima at the Holocene and the last interglacial, Nature, 589, 548–553, https://doi.org/10.1038/s41586-020-03155-x, 2021.

Brassell, S. C.: Application of biomarkers for delineating marine paleoclimatic fluctuations during the Pleistocene, Organic Geochemistry, 699–738, 1986.

Brierley, C. M., Zhao, A., Harrison, S. P., Braconnot, P., Williams, C. J. R., Thornalley, D. J. R., Shi, X., Peterschmitt, J.-Y., Ohgaito, R., Kaufman, D. S., Kageyama, M., Hargreaves, J. C., Erb, M. P., Emile-Geay, J., D'Agostino, R., Chandan, D., Carré, M., Bartlein, P. J., Zheng, W., Zhang, Z., Zhang, Q., Yang, H., Volodin, E. M., Tomas, R. A., Routson, C., Peltier, W. R., Otto-Bliesner, B., Morozova, P. A., McKay, N. P., Lohmann, G., Legrande, A. N., Guo, C., Cao, J., Brady, E., Annan, J. D., and Abe-Ouchi, A.: Large-scale features and evaluation of the PMIP4-CMIP6 <i>midHolocene</i> simulations, Climate of the Past, 16, 1847–1872, https://doi.org/10.5194/cp-16-1847-2020, 2020.

Brocas, W. M., Felis, T., and Mudelsee, M.: Tropical Atlantic Cooling and Freshening in the Middle of the Last Interglacial From Coral Proxy Records, Geophysical Research Letters, 46, 8289–8299, https://doi.org/10.1029/2019gl083094, 2019.

Chen, Y.-l. L., Chen, H.-Y., and Chung, C.-W.: Seasonal variability of coccolithophore abundance and assemblage in the northern South China Sea, Deep Sea Research Part II: Topical Studies in Oceanography, 54, 1617–1633, https://doi.org/10.1016/j.dsr2.2007.05.005, 2007.

Clement, A. C., Seager, R., and Cane, M. A.: Orbital controls on the El Niño/Southern Oscillation and the tropical climate, Paleoceanography, 14, 441–456, https://doi.org/10.1029/1999pa900013, 1999.

https://doi.org/10.5194/egusphere-2026-1891
Preprint. Discussion started: 15 April 2026

Conan, S. M. H. and Brummer, G. J. A.: Fluxes of planktic foraminifera in response to monsoonal upwelling on the Somalia Basin margin, Deep Sea Research Part II: Topical Studies in Oceanography, 47, 2207–2227, https://doi.org/10.1016/S0967-0645(00)00022-9, 2000.

Crow, B. R. and Prange, M.: Long- and short-term variability of Arctic sea-ice cover during the Last Interglacial and Marine Isotope Stage 11c, Communications Earth & Environment, 6, https://doi.org/10.1038/s43247-025-02267-4, 2025.

Crow, B. R., Prange, M., and Schulz, M.: Dynamic boreal summer atmospheric circulation response as negative feedback to Greenland melt during the MIS-11 interglacial, Climate of the Past, 18, 775–792, https://doi.org/10.5194/cp-18-775-2022, 2022.

Curry, W. B., Ostermann, D. R., Guptha, M. V. S., and Ittekkot, V.: Foraminiferal production and monsoonal upwelling in the Arabian Sea: evidence from sediment traps, Geological Society, London, Special Publications, 64, 93–106, https://doi.org/10.1144/GSL.SP.1992.064.01.06, 1992.

Dong, Y., Proistosescu, C., Armour, K. C., and Battisti, D. S.: Attributing Historical and Future Evolution of Radiative Feedbacks to Regional Warming Patterns using a Green's Function Approach: The Preeminence of the Western Pacific, Journal of Climate, 32, 5471–5491, https://doi.org/10.1175/jcli-d-18-0843.1, 2019.

Dupont, L.: Vegetation zones in NW Africa during the Brunhes chron reconstructed from marine palynological data, Quaternary Science Reviews, 12, 189–202, 10.1016/0277-3791(93)90053-O, 1993.

Dyez, K. A., Ravelo, A. C., and Mix, A. C.: Evaluating drivers of Pleistocene eastern tropical Pacific sea surface temperature, Paleoceanography, 31, 1054–1069, https://doi.org/10.1002/2015PA002873, 2016.

England, M. R., Polvani, L. M., Sun, L., and Deser, C.: Tropical climate responses to projected Arctic and Antarctic sea-ice loss, Nature Geoscience, 13, 275–281, https://doi.org/10.1038/s41561-020-0546-9, 2020.

Erfani, E. and Burls, N. J.: The Strength of Low-Cloud Feedbacks and Tropical Climate: A CESM Sensitivity Study, Journal of Climate, 32, 2497–2516, https://doi.org/10.1175/JCLI-D-18-0551.1, 2019.

Fan, L., Shin, S. I., Liu, Q., and Liu, Z.: Relative importance of tropical SST anomalies in forcing East Asian summer monsoon circulation, Geophysical Research Letters, 40, 2471–2477, https://doi.org/10.1002/grl.50494, 2013.

Fischer, H., Meissner, K. J., Mix, A. C., Abram, N. J., Austermann, J., Brovkin, V., Capron, E., Colombaroli, D., Daniau, A.-L., Dyez, K. A., Felis, T., Finkelstein, S. A., Jaccard, S. L., McClymont, E. L., Rovere, A., Sutter, J., Wolff, E. W., Affolter, S., Bakker, P., Ballesteros-Cánovas, J. A., Barbante, C., Caley, T., Carlson, A. E., Churakova, O., Cortese, G., Cumming, B. F., Davis, B. A. S., de Vernal, A., Emile-Geay, J., Fritz, S. C., Gierz, P., Gottschalk, J., Holloway, M. D., Joos, F., Kucera, M., Loutre, M.-F., Lunt, D. J., Marcisz, K., Marlon, J. R., Martinez, P., Masson-Delmotte, V., Nehrbass-Ahles, C., Otto-Bliesner, B. L., Raible, C. C., Risebrobakken, B., Sánchez Goñi, M. F., Arrigo, J. S., Sarnthein, M., Sjolte, J., Stocker, T. F., Velasquez Alvárez, P. A., Tinner, W., Valdes, P. J., Vogel, H., Wanner, H., Yan, Q., Yu, Z., Ziegler, M., and Zhou, L.: Palaeoclimate constraints on the impact of 2 °C anthropogenic warming and beyond, Nature Geoscience, 11, 474–485, https://doi.org/10.1038/s41561-018-0146-0, 2018.

Gagan, M. K., Hendy, E. J., Haberle, S. G., and Hantoro, W. S.: Post-glacial evolution of the Indo-Pacific Warm Pool and El Niño-Southern oscillation, Quaternary International, 118-119, 127–143, https://doi.org/10.1016/s1040-6182(03)00134-4, 2004.

Gebregiorgis, D., Hathorne, E. C., Giosan, L., Clemens, S., Nurnberg, D., and Frank, M.: Southern Hemisphere forcing of South Asian monsoon precipitation over the past ~1 million years, Nature communications, 9, 4702, https://doi.org/10.1038/s41467-018-07076-2, 2018.

Gray, W. R., Weldeab, S., Lea, D. W., Rosenthal, Y., Gruber, N., Donner, B., and Fischer, G.: The effects of temperature, salinity, and the carbonate system on Mg/Ca in Globigerinoides ruber (white): A global sediment trap calibration, Earth and Planetary Science Letters, 482, 607–620, https://doi.org/10.1016/j.epsl.2017.11.026, 2018.

Held, I. M. and Soden, B. J.: Robust Responses of the Hydrological Cycle to Global Warming, Journal of Climate, 19, 5686–5699, https://doi.org/10.1175/JCLI3990.1, 2006.

Hirahara, S., Ishii, M., and Fukuda, Y.: Centennial-scale sea surface temperature analysis and its uncertainty, Journal of Climate, 27, 57–75, https://doi.org/10.1175/JCLI-D-12-00837.1, 2014.

Hoffman, J. S., Clark, P. U., Parnell, A. C., and He, F.: Regional and global sea-surface temperatures during the last interglaciation, Science, 355, 276–279, https://doi.org/10.1126/science.aai8464, 2017.

Hollstein, M., Mohtadi, M., Kienast, M., Rosenthal, Y., Groeneveld, J., Oppo, D. W., Southon, J. R., and Lückge, A.: The Impact of Astronomical Forcing on Surface and Thermocline Variability Within the Western Pacific Warm Pool Over the Past 160 kyr, Paleoceanography and Paleoclimatology, 35, https://doi.org/10.1029/2019pa003832, 2020.

Hurrell, J. W., Holland, M. M., Gent, P. R., Ghan, S., Kay, J. E., Kushner, P. J., Lamarque, J. F., Large, W. G., Lawrence, D., Lindsay, K., Lipscomb, W. H., Long, M. C., Mahowald, N., Marsh, D. R., Neale, R. B., Rasch, P., Vavrus, S., Vertenstein, M., Bader, D., Collins, W. D., Hack, J. J., Kiehl, J., and Marshall, S.: The Community Earth System Model: A Framework for Collaborative Research, Bulletin of the American Meteorological Society, 94, 1339–1360, https://doi.org/10.1175/bams-d-12-00121.1, 2013.

Jia, Q., Li, T., Xiong, Z., Steinke, S., Jiang, F., Chang, F., and Qin, B.: Hydrological variability in the western tropical Pacific over the past 700 kyr and its linkage to Northern Hemisphere climatic change, Palaeogeography, Palaeoclimatology, Palaeoecology, 10.1016/j.palaeo.2017.12.039, 2018.

Jian, Z., Wang, Y., Dang, H., Mohtadi, M., Rosenthal, Y., Lea, D. W., Liu, Z., Jin, H., Ye, L., Kuhnt, W., and Wang, X.: Warm pool ocean heat content regulates ocean–continent moisture transport, Nature, 612, 92–99, https://doi.org/10.1038/s41586-022-05302-y, 2022.

Jonkers, L., Hollstein, M., Siccha, M., and Kucera, M.: The PALMOD 130k marine palaeoclimate data synthesis version 2, Earth System Science Data, accepted.

https://doi.org/10.5194/egusphere-2026-1891
Preprint. Discussion started: 15 April 2026

Kaufman, D. S. and Broadman, E.: Revisiting the Holocene global temperature conundrum, Nature, 614, 425–435, https://doi.org/10.1038/s41586-022-05536-w, 2023.
Kaufman, D. S., McKay, N., Routson, C., Erb, M., Davis, B., Heiri, O., Jaccard, S., Tierney, J., Datwyler, C., Axford, Y., Brussel, T., Cartapanis, O., Chase, B., Dawson, A., de Vernal, A., Engels, S., Jonkers, L., Marsicek, J., Moffa-Sanchez, P., Morrill, C., Orsi, A., Rehfeld, K., Saunders, K., Sommer, P. S., Thomas, E., Tonello, M., Toth, M., Vachula, R., Andreev, A., Bertrand, S., Biskaborn, B., Bringue, M., Brooks, S., Caniupan, M., Chevalier, M., Cwynar, L., Emile-Geay, J., Fegyveresi, J., Feurdean, A., Finsinger, W., Fortin, M. C., Foster, L., Fox, M., Gajewski, K., Grosjean, M., Hausmann, S., Heinrichs, M., Holmes, N., Ilyashuk, B., Ilyashuk, E., Juggins, S., Khider, D., Koinig, K., Langdon, P., Larocque-Tobler, I., Li, J., Lotter, A., Luoto, T., Mackay, A., Magyari, E., Malevich, S., Mark, B., Massaferro, J., Montade, V., Nazarova, L., Novenko, E., Paril, P., Pearson, E., Peros, M., Pienitz, R., Plociennik, M., Porinchu, D., Potito, A., Rees, A., Reinemann, S., Roberts, S., Rolland, N., Salonen, S., Self, A., Seppa, H., Shala, S., St-Jacques, J. M., Stenni, B., Syrykh, L., Tarrats, P., Taylor, K., van den Bos, V., Velle, G., Wahl, E., Walker, I., Wilmshurst, J., Zhang, E., and Zhilich, S.: A global database of Holocene paleotemperature records, Scientific data, 7, 115, https://doi.org/10.1038/s41597-020-0445-3, 2020.
Kawahata, H., Nishimura, A., and Gagan, M. K.: Seasonal change in foraminiferal production in the western equatorial Pacific warm pool: evidence from sediment trap experiments, Deep-Sea Research Part II: Topical Studies in Oceanography, 49, 2783–2800, https://doi.org/10.1016/S0967-0645(02)00058-9, 2002.
Kincaid, E., Thunell, R. C., Le, J., Lange, C. B., Weinheimer, A. L., and Reid, F. M. H.: Planktonic foraminiferal fluxes in the Santa Barbara Basin: response to seasonal and interannual hydrographic changes, Deep Sea Research Part II: Topical Studies in Oceanography, 47, 1157–1176, https://doi.org/10.1016/S0967-0645(99)00140-X, 2000.
Kleinen, T., Hildebrandt, S., Prange, M., Rachmayani, R., Müller, S., Bezrukova, E., Brovkin, V., and Tarasov, P. E.: The climate and vegetation of Marine Isotope Stage 11 – Model results and proxy-based reconstructions at global and regional scale, Quaternary International, 348, 247–265, https://doi.org/10.1016/j.quaint.2013.12.028, 2014.
Koutavas, A., Lynch-Stieglitz, J., Marchitto, T. M., and Sachs, J. P.: El Nino-like pattern in ice age tropical Pacific sea surface temperature, Science, 297, 226–230, https://doi.org/10.1126/science.1072376, 2002.
Langner, M. and Mulitza, S.: Technical note: PaleoDataView – a software toolbox for the collection, homogenization and visualization of marine proxy data, Climate of the Past, 15, 2067–2072, https://doi.org/10.5194/cp-15-2067-2019, 2019.
Laskar, J., Robutel, P., Joutel, F., Gastineau, M., Correia, A. C. M., and Levrard, B.: A long term numerical solution for the insolation quantities of the Earth, Astronomy and Astrophysics, 428, 261–285, https://doi.org/10.1051/0004-6361:20041335, 2004.
Leduc, G., Schneider, R., Kim, J. H., and Lohmann, G.: Holocene and Eemian sea surface temperature trends as revealed by alkenone and Mg/Ca paleothermometry, Quaternary Science Reviews, 29, 989–1004, https://doi.org10.1016/j.quascirev.2010.01.004, 2010.
Lin, H.-L., Wang, W.-C., and Hung, G.-W.: Seasonal variation of planktonic foraminiferal isotopic composition from sediment traps in the South China Sea, Marine Micropaleontology, 53, 447–460, https://doi.org/10.1016/j.marmicro.2004.08.004, 2004.
Lisiecki, L. E. and Raymo, M. E.: A Pliocene-Pleistocene stack of 57 globally distributed benthic $\delta^{18}O$ records, Paleoceanography, 20, https://doi.org/10.1029/2004pa001071, 2005.
Liu, W., Xie, S.-P., Liu, Z., and Zhu, J.: Overlooked possibility of a collapsed Atlantic Meridional Overturning Circulation in warming climate, Science Advances, 3, e1601666, https://doi.org/10.1126/sciadv.1601666, 2017.
Liu, Y., Zhang, M., Liu, Z., Xia, Y., Huang, Y., Peng, Y., and Zhu, J.: A Possible Role of Dust in Resolving the Holocene Temperature Conundrum, Scientific reports, 8, 4434, https://doi.org/10.1038/s41598-018-22841-5, 2018.
Liu, Z., Zhu, J., Rosenthal, Y., Zhang, X., Otto-Bliesner, B. L., Timmermann, A., Smith, R. S., Lohmann, G., Zheng, W., and Elison Timm, O.: The Holocene temperature conundrum, Proceedings of the National Academy of Sciences of the United States of America, 111, E3501–3505, https://doi.org/10.1073/pnas.1407229111, 2014.
Lo, L., Shen, C.-C., Zeeden, C., Tsai, Y.-H., Yin, Q., Yang, C.-C., Chang, T.-L., Su, Y.-C., Mii, H.-S., Chuang, C.-K., and Chen, Y.-C.: Orbital control on the thermocline structure during the past 568 kyr in the Solomon Sea, southwest equatorial Pacific, Quaternary Science Reviews, 295, https://doi.org/10.1016/j.quascirev.2022.107756, 2022.
Lohmann, G., Pfeiffer, M., Laepple, T., Leduc, G., and Kim, J. H.: A model–data comparison of the Holocene global sea surface temperature evolution, Climate of the Past, 9, 1807–1839, 10.5194/cp-9-1807-2013, 2013.
Lu, Z., Liu, Z., Chen, G., and Guan, J.: Prominent Precession Band Variance in ENSO Intensity Over the Last 300,000 Years, Geophysical Research Letters, 46, 9786–9795, https://doi.org/10.1029/2019GL083410, 2019.
Lückge, A., Mohtadi, M., Rühlemann, C., Scheeder, G., Vink, A., Reinhardt, L., and Wiedicke, M.: Monsoon versus ocean circulation controls on paleoenvironmental condition off southern Sumatra during the past 300,000 years, Paleoceanography, 24, https://doi.org/10.1029/2008PA001627, 2009.
Mantsis, D. F., Clement, A. C., Broccoli, A. J., and Erb, M. P.: Climate Feedbacks in Response to Changes in Obliquity, Journal of Climate, 24, 2830–2845, https://doi.org/10.1175/2010jcli3986.1, 2011.
Marchitto, T. M., Muscheler, R., Ortiz, J. D., Carriquiry, J. D., and van Geen, A.: Dynamical Response of the Tropical Pacific Ocean to Solar Forcing During the Early Holocene, Science, 330, 1378–1381, https://doi.org/10.1126/science.1194887, 2010.
McKay, N., Overpeck, J. T., and Otto-Bliesner, B.: The role of ocean thermal expansion in Last Interglacial sea level rise, Geophysical Research Letters, 38, https://doi.org10.1029/2011GL048280, 2011.
Members:, C.-L. I. P.: Last Interglacial Arctic warmth confirms polar amplification of climate change, Quaternary Science Reviews, 25, 1383–1400, 2006.
Milker, Y., Rachmayani, R., Weinkauf, M. F. G., Prange, M., Raitzsch, M., Schulz, M., and Kučera, M.: Global and regional sea surface temperature trends during Marine Isotope Stage 11, Climate of the Past, 9, 2231–2252, https://doi.org/10.5194/cp-9-2231-2013, 2013.

https://doi.org/10.5194/egusphere-2026-1891
Preprint. Discussion started: 15 April 2026

Mohtadi, M., Oppo, D. W., Lückge, A., DePol-Holz, R., Steinke, S., Groeneveld, J., Hemme, N., and Hebbeln, D.: Reconstructing the thermal structure of the upper ocean: Insights from planktic foraminifera shell chemistry and alkenones in modern sediments of the tropical eastern Indian Ocean, Paleoceanography, 26, https://doi.org/10.1029/2011pa002132, 2011.
Mohtadi, M., Steinke, S., Groeneveld, J., Fink, H. G., Rixen, T., Hebbeln, D., Donner, B., and Herunadi, B.: Low-latitude control on seasonal and interannual changes in planktonic foraminiferal flux and shell geochemistry off south Java: A sediment trap study, Paleoceanography, 24, https://doi.org/10.1029/2008pa001636, 2009.
Morard, R., Fullberg, A., Brummer, G. A., Greco, M., Jonkers, L., Wizemann, A., Weiner, A. K. M., Darling, K., Siccha, M., Ledevin, R., Kitazato, H., de Garidel-Thoron, T., de Vargas, C., and Kucera, M.: Genetic and morphological divergence in the warm-water planktonic foraminifera genus Globigerinoides, PloS one, 14, e0225246, https://doi.org/10.1371/journal.pone.0225246, 2019.
Nascimento, R. A., Johnstone, H. J. H., Kuhnert, H., Santos, T. P., Venancio, I. M., Chiessi, C. M., Ballalai, J. M., Campos, M. C., Govin, A., Mulitza, S., and Albuquerque, A. L. S.: Long-term variability of the western tropical Atlantic sea surface temperature driven by greenhouse gases and AMOC, Quaternary Science Reviews, 322, https://doi.org/10.1016/j.quascirev.2023.108431, 2023.
Nascimento, R. A., Shimizu, M. H., Venancio, I. M., Chiessi, C. M., Kuhnert, H., Johnstone, H. J. H., Govin, A., Lessa, D., Ballalai, J. M., Santos, T. P., Piacsek, P., Mulitza, S., and Albuquerque, A. L. S.: Warmer western tropical South Atlantic during the Last Interglacial relative to the current interglacial period, Global and Planetary Change, 215, https://doi.org/10.1016/j.gloplacha.2022.103889, 2022.
Neale, R. and Slingo, J.: The Maritime Continent and Its Role in the Global Climate: A GCM Study, Journal of Climate, 16, 834–848, https://doi.org/10.1175/1520-0442(2003)016<0834:TMCAIR>2.0.CO;2, 2003.
Otto-Bliesner, B. L., Brady, E. C., Zhao, A., Brierley, C., Axford, Y. L., Capron, E., Govin, A., Hoffman, J. S., Isaacs, E., and Kageyama, M.: Large-scale features of Last Interglacial climate: Results from evaluating the lig127k simulations for the Coupled Model Intercomparison Project (CMIP6)-Paleoclimate Modeling Intercomparison Project (PMIP4), Climate of the Past, 17, 63–94, https://doi.org/10.5194/cp-17-63-2021, 2021.
Otto-Bliesner, B. L., Braconnot, P., Harrison, S. P., Lunt, D. J., Abe-Ouchi, A., Albani, S., Bartlein, P. J., Capron, E., Carlson, A. E., Dutton, A., Fischer, H., Goelzer, H., Govin, A., Haywood, A., Joos, F., LeGrande, A. N., Lipscomb, W. H., Lohmann, G., Mahowald, N., Nehrbass-Ahles, C., Pausata, F. S. R., Peterschmitt, J.-Y., Phipps, S. J., Renssen, H., and Zhang, Q.: The PMIP4 contribution to CMIP6 – Part 2: Two interglacials, scientific objective and experimental design for Holocene and Last Interglacial simulations, Geoscientific Model Development, 10, 3979–4003, https://doi.org/10.5194/gmd-10-3979-2017, 2017.
PAGES, P. I. W. g. o.: Interglacials of the last 800,000 years, Reviews of Geophysics, 54, 162–219, https://doi.org/10.1002/2015RG000482, 2016.
Pena, L. D., Cacho, I., Ferretti, P., and Hall, M. A.: El Niño-Southern Oscillation-like variability during glacial terminations and interlatitudinal teleconnections, Paleoceanography, 23, n/a–n/a, https://doi.org/10.1029/2008pa001620, 2008.
Qu, T., Gao, S., and Fine, R. A.: Subduction of South Pacific Tropical Water and its equatorward pathways as shown by a simulated passive tracer, Journal of Physical Oceanography, 43, 1551–1565, https://doi.org/doi:10.1175/jpo-d-12-0180.1, 2013.
Rosenthal, Y., Boyle, E. A., and Slowey, N.: Temperature control on the incorporation of magnesium, strontium, fluorine, and cadmium into benthic foraminiferal shells from Little Bahama Bank: Prospects for thermocline paleoceanography, Geochimica Et Cosmochimica Acta, 61, 3633–3643, https://doi.org/10.1016/S0016-7037(97)00181-6, 1997.
Sagawa, T., Okamura, K., and Murayama, M.: Orbital-scale thermocline temperature variability in the western equatorial Pacific during the last 370 kyr, Palaeogeography, Palaeoclimatology, Palaeoecology, 608, 111285, https://doi.org/10.1016/j.palaeo.2022.111285, 2022.
Schneider, B., Leduc, G., and Park, W.: Disentangling seasonal signals in Holocene climate trends by satellite-model-proxy integration, Paleoceanography, 25, n/a–n/a, 10.1029/2009pa001893, 2010.
Soden, B. J. and Held, I. M.: An assessment of climate feedbacks in coupled ocean-atmosphere models, Journal of Climate, 19, 3354–3360, https://doi.org/10.1175/JCLI3799.1, 2006.
Tachikawa, K., Timmermann, A., Vidal, L., Sonzogni, C., and Timm, O. E.: CO_2 radiative forcing and Intertropical Convergence Zone influences on western Pacific warm pool climate over the past 400 ka, Quaternary Science Reviews, 86, 24–34, https://doi.org/10.1016/j.quascirev.2013.12.018, 2014.
Thompson, A. J., Zhu, J., Poulsen, C. J., Tierney, J. E., and Skinner, C. B.: Northern Hemisphere vegetation change drives a Holocene thermal maximum, Science Advances, 8, https://doi.org/10.1126/sciadv.abj6535, 2022.
Tierney, J. E. and Tingley, M. P.: BAYSPLINE: A New Calibration for the Alkenone Paleothermometer, Paleoceanography and Paleoclimatology, 33, 281–301, https://doi.org/10.1002/2017PA003201, 2018.
Timmermann, A., Sachs, J., and Timm, O. E.: Assessing divergent SST behavior during the last 21 ka derived from alkenones and *G. ruber*-Mg/Ca in the equatorial Pacific, Paleoceanography, 29, 680–696, https://doi.org/10.1002/2013pa002598, 2014a.
Timmermann, A., Friedrich, T., Timm, O. E., Chikamoto, M. O., Abe-Ouchi, A., and Ganopolski, A.: Modeling obliquity and CO_2 effects on southern hemisphere climate during the Past 408 ka, Journal of Climate, 27, 1863–1875, https://doi.org/10.1175/jcli-d-13-00311.1, 2014b.
Toggweiler, J. R. and Si, W.: A New Role for the AMOC During the Ice Ages, Paleoceanography and Paleoclimatology, 40, e2024PA004973, https://doi.org/10.1029/2024PA004973, 2025.
Turney, C. S. M., Jones, R. T., McKay, N. P., Van Sebille, E., Thomas, Z., Hillenbrand, C.-D., and Fogwill, C. J.: A global mean sea surface temperature dataset for the Last Interglacial (129–116 ka) and contribution of thermal expansion to sea level change, Earth System Science Data, 12, 3341–3356, https://doi.org/10.5194/essd-12-3341-2020, 2020.

https://doi.org/10.5194/egusphere-2026-1891
Preprint. Discussion started: 15 April 2026

Wang, H. and Mehta, V. M.: Decadal Variability of the Indo-Pacific Warm Pool and Its Association with Atmospheric and Oceanic Variability in the NCEP–NCAR and SODA Reanalyses, Journal of Climate, 21, 5545–5565, https://doi.org/10.1175/2008jcli2049.1, 2008.

Wang, Y., Jian, Z., Zhao, P., Chen, J. F., and Xiao, D.: Precessional forced evolution of the Indian Ocean Dipole, Journal of Geophysical Research: Oceans, 120, 3747–3760, https://doi.org/10.1002/2015jc010713, 2015.

Wang, Y. V., Leduc, G., Regenberg, M., Andersen, N., Larsen, T., Blanz, T., and Schneider, R. R.: Northern and southern hemisphere controls on seasonal sea surface temperatures in the Indian Ocean during the last deglaciation, Paleoceanography, 28, 619–632, https://doi.org/10.1002/palo.20053, 2013.

Watanabe, M., Iwakiri, T., Dong, Y., and Kang, S. M.: Two Competing Drivers of the Recent Walker Circulation Trend, Geophysical Research Letters, 50, e2023GL105332, https://doi.org/10.1029/2023GL105332, 2023.

Yamasaki, M., Sasaki, A., Oda, M., and Domitsu, H.: Western equatorial Pacific planktic foraminiferal fluxes and assemblages during a La Niña year (1999), Marine Micropaleontology, 66, 304–319, https://doi.org/10.1016/j.marmicro.2007.10.006, 2008.

Yin, Q. Z. and Berger, A.: Individual contribution of insolation and CO2 to the interglacial climates of the past 800,000 years, Clim Dynam, 38, 709–724, https://doi.org/10.1007/s00382-011-1013-5, 2011.

Zelinka, M. D., Myers, T. A., McCoy, D. T., Po-Chedley, S., Caldwell, P. M., Ceppi, P., Klein, S. A., and Taylor, K. E.: Causes of Higher Climate Sensitivity in CMIP6 Models, Geophysical Research Letters, 47, 10.1029/2019gl085782, 2020.

Zhang, Q., Sundqvist, H. S., Moberg, A., Körnich, H., Nilsson, J., and Holmgren, K.: Climate change between the mid and late Holocene in northern high latitudes – Part 2: Model-data comparisons, Clim. Past, 6, 609–626, https://doi.org/10.5194/cp-6-609-2010, 2010.

Zhang, S., Yu, Z., Gong, X., Wang, Y., Chang, F., Lohmann, G., Qi, Y., and Li, T.: Precession cycles of the El Niño/Southern oscillation-like system controlled by Pacific upper-ocean stratification, Communications Earth & Environment, 2, https://doi.org/10.1038/s43247-021-00305-5, 2021.